Chapter 5
Dark Current-Voltage Characterization

Dark current-voltage (IV) response determines electrical performance of the solar cell without light illumination. Dark IV measurement (Fig. 5.1) carries no information on either short-circuit current (I_{SC}) or open-circuit voltage (V_{OC}), yet reliable and accurate information regarding other parameters including series resistance, shunt resistance, diode factor, and diode saturation currents is gained; diode parameters are instrumental in estimating solar cell efficiency. Ideal dark IV response in Fig. 5.1a reveals negligible current flow at voltages lower than the turn-on voltage. At higher voltages, large current flows through the forward-biased diode. In practice, it is useful to plot diode IV response on logarithmic scale in order to define series and shunt resistance measurement regions (Fig. 5.1b). The reader is referred to references [1–9] for theoretical basis and parametric model extraction. This chapter applies dark IV method to determine electrical characteristics of ohmic and rectifying contacts to n- and p-doped Si wafers. A brief PC1D-based simulation of I-V response as a function of relevant process parameters is followed by description of measurement methodology and experimental results on screen-printed Al and Ag paste contacts to solar cells.

5.1 PC1D Current-Voltage Simulations

PC1D software simulations have been used extensively in this book and elsewhere for accurate solar cell analysis. This software is used to determine I-V response for both n- and p-type Si wafers.

S. H. Zaidi, *Crystalline Silicon Solar Cells*,
https://doi.org/10.1007/978-3-030-73379-7_5

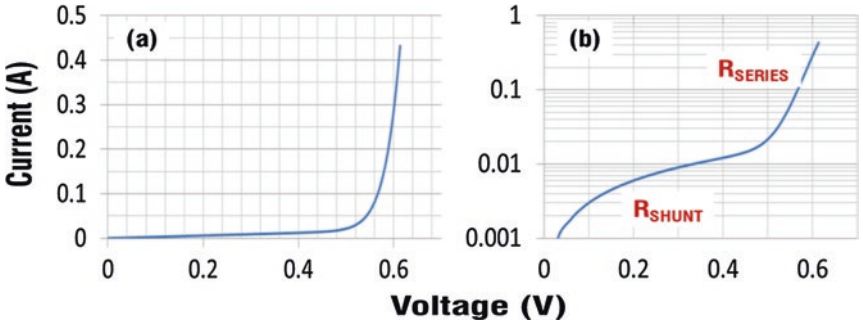

Fig. 5.1 Simulated current versus voltage responses of 18% efficient solar cell on linear (left) and logarithmic (right) scales

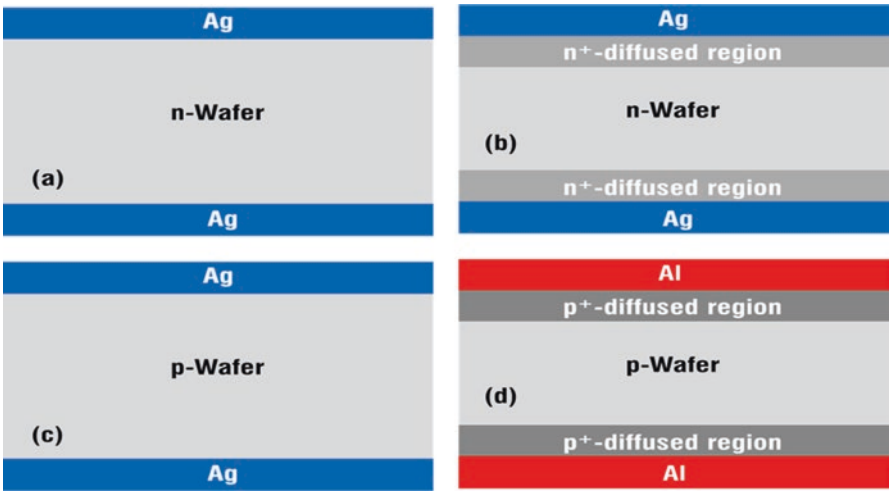

Fig. 5.2 Ag and Al contact configurations on n- and p-doped Si wafers

5.1.1 Ohmic Contacts

In solar cells, Ag and Al contacts are formed to doped (n-type) and un-doped (p-type) surfaces, respectively, to form negative and positive contacts. Figure 5.2 illustrates typical configurations in solar cell processing. Configurations in Figs. 5.2b and d relate to ohmic contacts on front and rear surfaces of monofacial solar cells; for convenience, anti-reflection and passivation films have been omitted. Configurations in Figs. 5.2a and c are unusual and have been included only for instructional purposes. PC1D software is not designed to simulate contacts to un-doped surfaces; experimental data will be used to illustrate I-V response of these surfaces. Figure 5.3 plots simulated I-V response of Ag or Al contacts as a function

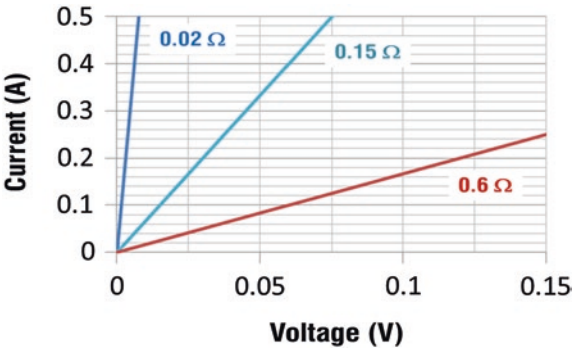

Fig. 5.3 Current-voltage responses of ohmic contacts as a function of series resistance

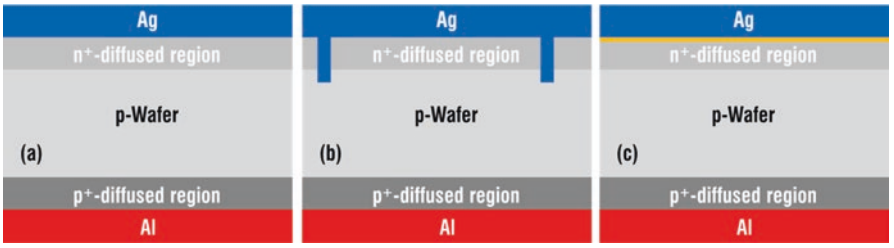

Fig. 5.4 Description of ideal (**a**) and nonideal diode configurations illustrating enhanced shunting (**b**) high series resistance (**c**)

of cumulative series resistance. Current-voltage response is ohmic and nearly vertical for low resistances and horizontal for high resistances.

5.1.2 Rectifying Contacts

For the purpose of simulations, rectifying contacts are $n^+/p/p^+$ diodes illustrated in Fig. 5.4 for ideal and nonideal cases. In the ideal configuration (Fig. 5.4a), contacts and related solar cell parameters are optimized to 18% efficiency. In nonideal cases, all parameters are kept optimal except shunt (Fig. 5.4b) and series (Fig. 5.4c) resistances. These process imperfections lower solar cell efficiency. In solar cells, highest efficiency requires shallow emitters. However, high temperature annealing can cause spikes of Ag across the emitter region to form contact with the p-type substrate and shunting the solar cell. Similarly, if the process temperature is lower than optimal or the paste does not completely etch the anti-reflection SiN or SiO_2 film, a barrier is formed at the Ag/n-Si interface that increases series resistance. Figure 5.5 displays I-V response, on linear and logarithmic scale, of 18% efficient solar cell as its shunt resistance is reduced from ~33 Ω to 1.5 Ω. As shunt resistance increases, diode loses its rectifying characteristics and eventually becomes a resistor. Figure 5.6 simulates solar cell response as a function of series resistance in 0.015–0.6-Ω range.

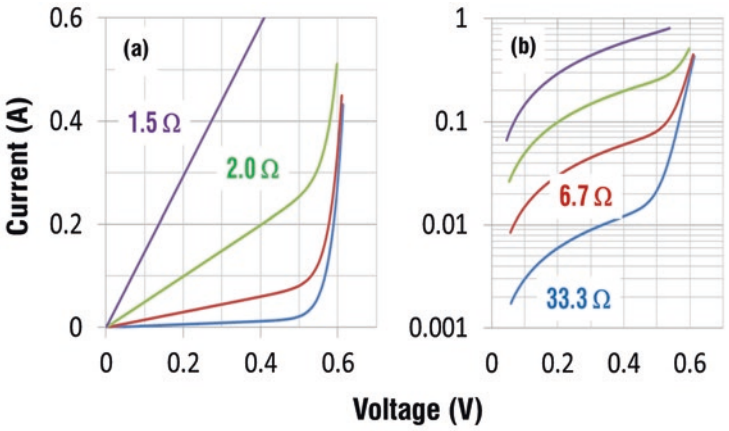

Fig. 5.5 Current-voltage simulations of dark IV diodes plotted as a function of shunt resistances on linear (**a**) and logarithmic (**b**) scales; for comparison ideal diode response has also been included

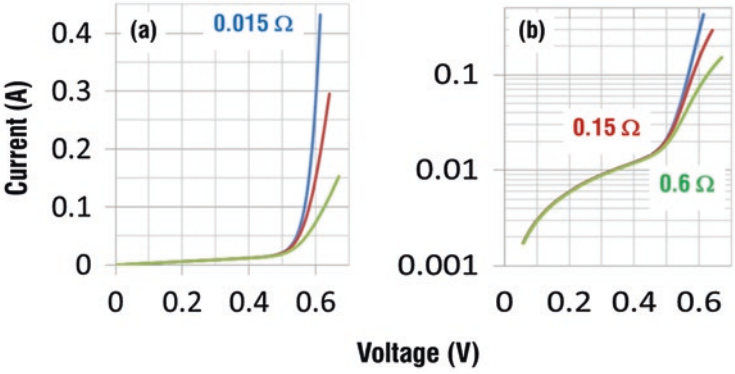

Fig. 5.6 Current-voltage simulations of dark IV diodes plotted as a function of series resistances on linear (**a**) and logarithmic (**b**) scales; for comparison ideal diode response has also been included

Based on Ohm's law, the current flow will decrease as resistance is increased; therefore, solar cells with high series resistance will exhibit low photo-generated current.

The most important parameter in limiting solar cell efficiency is its minority carrier lifetime. Dark I-V simulations were also investigated as a function of carrier lifetime. Figure 5.7 plots dark I-V responses for lifetimes in 10–1000-μsec range. For these simulations, all other process parameters were kept identical. It is noted that diode turn-on voltage is reduced as lifetime is reduced. Industrially produced monofacial solar cells are fabricated on wafers with lifetimes in ~10–20-μsec range; highest lifetime wafers are used for back contact solar cells.

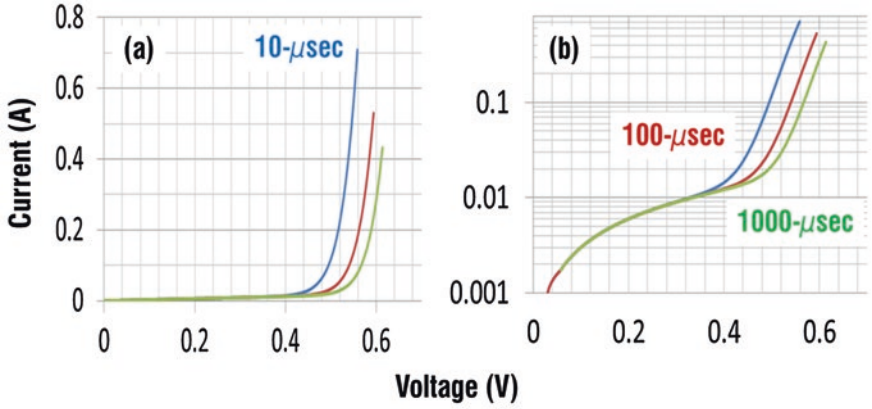

Fig. 5.7 Current-voltage simulations of dark IV diodes plotted as a function of minority carrier lifetime on linear (**a**) and logarithmic (**b**) scales; for comparison ideal diode response has also been included

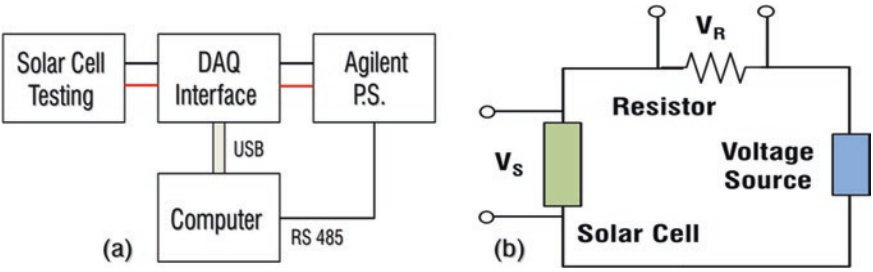

Fig. 5.8 Schematic diagrams of IV measurement system illustrating concept (**a**) and the circuit (**b**)

5.2 Measurement Methodology

A custom-designed current-voltage measurement system was developed and used for all measurements presented here. Figure 5.8 illustrates system circuit diagram. A programmable Agilent power supply is used to precisely vary voltage across the cell, while voltage across and current through it are simultaneously measured. LabVIEW software is used to measure solar cell current and voltage; acquired data is stored and plotted in real time. Figure 5.9 displays pictures of a solar cell under measurement including its IV response under illumination (Fig. 5.9a).

In order to independently establish validity of IV measurements, three commercial, SiN-coated solar cells (14% mc-Si, (b) 16% bifacial c-Si, and (c) 18% c-Si) with efficiencies in 14%–18% range were characterized. Figure 5.10 plots dark IV measurements from the three solar cells. It is noted that turn-on voltage is highest for 18% solar cell on account of its highest lifetime; plotted data is in good agreement with simulated data in Fig. 5.7. Due to voltage resolution limit of the

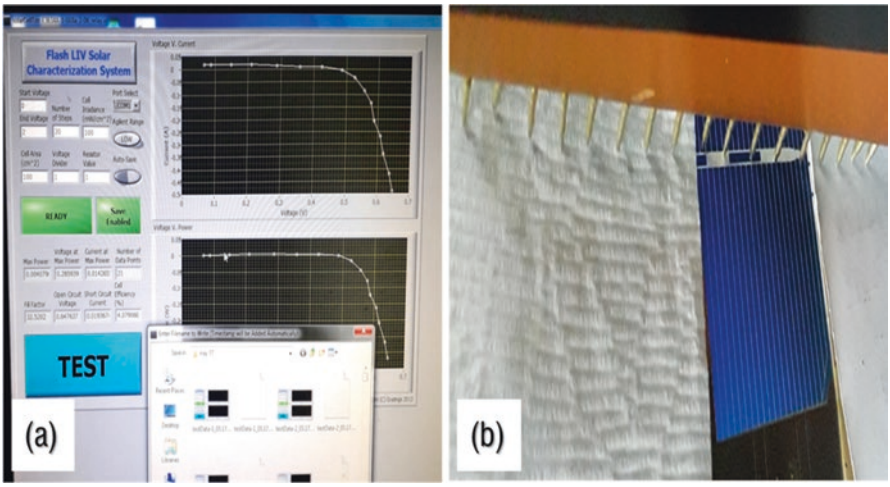

Fig. 5.9 Pictures of dark IV measurement system exhibiting measured and plotted I-V response (**a**) and 18% efficiency commercial SiN solar cell under test (**b**)

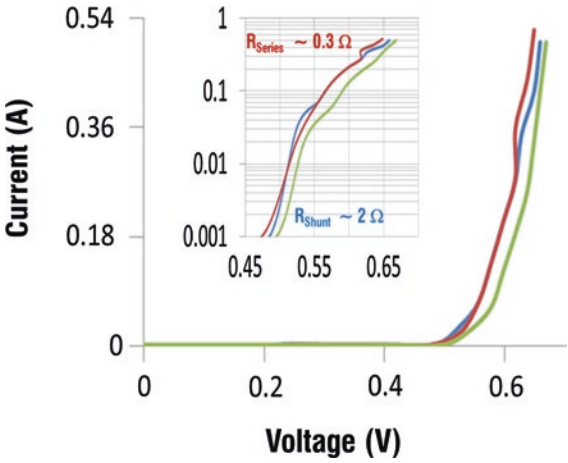

Fig. 5.10 Dark current-voltage measurements of commercial SiN-coated solar cells with efficiencies in 14–16% range exhibiting comparable series and shunt resistances; inset displays the same measurements on logarithmic scale

measurement system, current below 1 mA could not be detected. Therefore, shunt resistance measurements are not accurate especially for high-efficiency solar cells. However, with solar cell under illumination, shunt resistance can be easily measured and will be reported in the final chapter. In all subsequent measurements, IV response of 18% solar cell is used as a calibration standard in order to evaluate performance of solar cells fabricated as part of the author's research work.

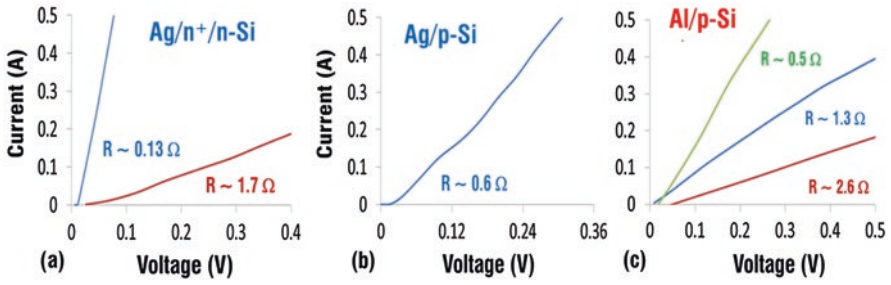

Fig. 5.11 Dark IV measurements from Ag and Al paste contacts on Si wafers showing linear ohmic response for (**a**) Ag on n^+ −doped n-Si, (**b**) Ag on un-doped p-Si, and (**c**) Al on p-Si

5.2.1 Current-Voltage Measurements on Ohmic Contacts

Figure 5.11 plots IV measurements of thermally annealed screen-printed Ag and Al paste contacts on un-doped n- and p-type wafers. Succinct features of ohmic contact measurements are summarized below.

(i) Ag contact resistance on n-Si wafer is a function of its doping. Without n^+-doping, no measurable current flow is detected within 0–0.4-V range. On doped n^+/n-Si wafers, Ag contact resistance varies from 0.13 Ω to 1.7 Ω as sheet resistance varies from ~20 Ω/square to 100 Ω/square range.
(ii) Ag on un-doped p-Si wafer forms ohmic contact with resistance of ~0.6 Ω.
(iii) Al contact resistance on un-doped p-Si wafer is a strong function of annealing temperature with lower resistance at higher temperatures related to formation of Al-Si alloyed regions described in Chap. 4.

Overall, dark IV measurements are in good agreement with simulations. Inability to reach zero current at zero voltage may be attributed to lack of resolution at voltages close to zero.

5.2.2 Current-Voltage Measurements on Rectifying Contacts

Dark I-V measurements from solar cells processed at higher than optimal temperatures exhibited characteristics similar to PC1D simulations (Fig. 5.12). Due to significantly higher current flow caused by shunting through 50 Ω/square emitter, measurement system was able to characterize both series and shunt resistances. Measured I-V responses at shunt resistances of 5 Ω and 1.7 Ω were in good agreement with simulated I-V responses at 6.7 Ω and 2 Ω in Fig. 5.5. At highest temperatures, IV response is practically a straight line with resistance of ~0.5 Ω.

At lower than optimal temperatures, contact resistivity is higher and is reflected in the dark I-V measurements plotted in Fig. 5.13. There is a good agreement with

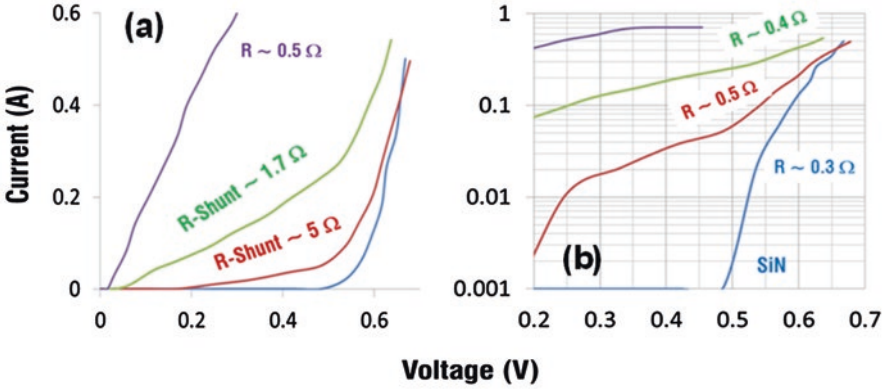

Fig. 5.12 Dark IV measurements from processed solar cells at temperatures higher than optimal: (**a**) exhibiting increasing lower shunt resistances on linear scale and (**b**) same measurements on logarithmic scale; for reference, IV response from 18% solar cell (blue line) has been included

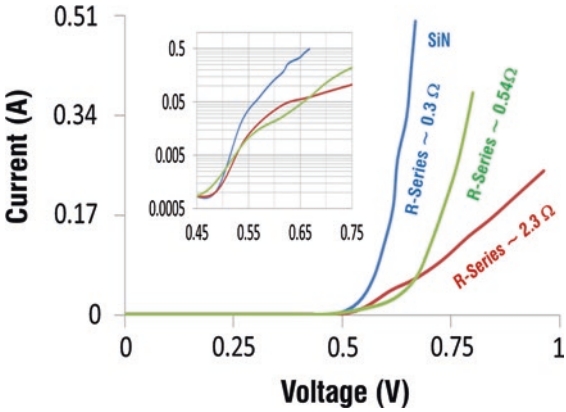

Fig. 5.13 Dark IV measurements from processed solar cells at lower than optimal temperatures exhibiting increasing series resistances; inset in the graph plots the same measurements at logarithmic scale; for reference, IV response from 18% solar cell (blue line) has been included

the simulated for 0.6 Ω series resistance in Fig. 5.6. Also, note that shunt response of all solar cells is nominally the same.

5.2.3 Current-Voltage Response Variation with Annealing Configurations

Chapter 4 described four thermal annealing configurations for screen-printed Ag and Al paste contacts in TLM configuration. In solar cells, the current flow is vertical; therefore, effectiveness of annealing configuration is evaluated through diode IV measurements. Simultaneous thermal annealing of Ag and Al paste contacts to

n-Si (front surface) and p-Si (rear surface) surfaces was carried out to determine optimum profiles for each system; optimum results for each case are discussed below.

Conveyor Belt IR RTA

Figure 5.14 plots dark IV diode response for simultaneously annealed Ag and Al contacts in conventional IR conveyor belt furnace. Comparison with 18% commercial solar cell reveals almost identical series and shunt resistances. Slight increase in diode turn-on voltage is attributed to variations in materials and processes. This temperature profile was used for annealing of different kinds of solar cells presented in Chap. 6.

Parallel-Plate RTA

Figure 5.15 plots diode IV response of Ag and Al contacts simultaneously annealed in parallel-plate configuration described in Chap. 4. In comparison with reference 18% cell, series resistance is slightly higher, while the shunt resistance is significantly lower. Comparison of series resistances in Figs. 5.14 and 5.15 reveals that both systems are able to form contacts with series resistance comparable to 18% efficient solar cell. Slightly lower shunt resistance in parallel-plate configuration is presumably due to light absorption from the quartz halogen lamps; this absorption mechanism can be controlled with optical filters.

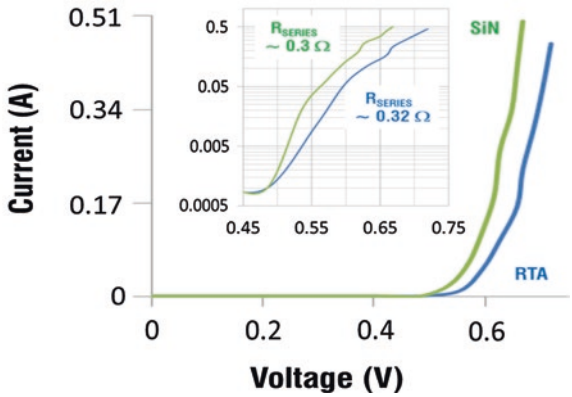

Fig. 5.14 Dark I-V measurements from processed solar cells at optimum temperature profile, in conventional IR conveyor belt furnace, exhibiting comparable series and shunt resistances to the commercial solar cell; inset in the graph plots the same measurements at logarithmic scale; for reference, IV response from 18% solar cell (blue line) has been included

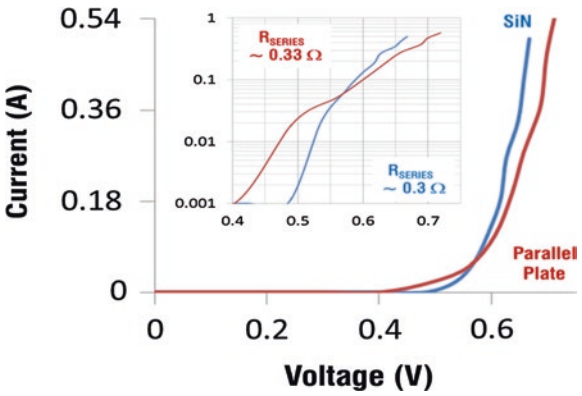

Fig. 5.15 Dark I-V measurements from processed solar cells at optimum temperature profile, in parallel-plate configuration, exhibiting slightly higher series and lower shunt resistances; inset in the graph plots the same measurements at logarithmic scale; for reference, I-V response from 18% solar cell (blue line) has been included

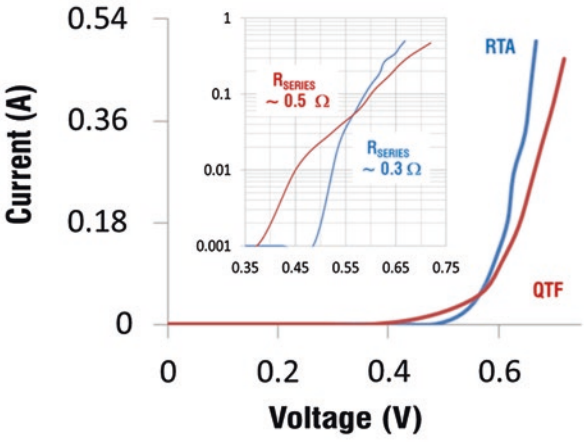

Fig. 5.16 Dark IV measurements from processed solar cells at optimum temperature profile, in quartz tube furnace, exhibiting higher series and lower shunt resistances; inset in the graph plots the same measurements at logarithmic scale; for reference, IV response from 18% solar cell has been included

Quartz Tube Furnace Anneal

Figure 5.16 displays dark IV measurements from Ag and Al contacts annealed simultaneously in quartz tube furnace described in Chap. 4. Comparison with 18% cell reveals that series resistance is high and shunt resistance is lower, thereby making this annealing configuration unsuitable for simultaneous annealing of solar cell contacts.

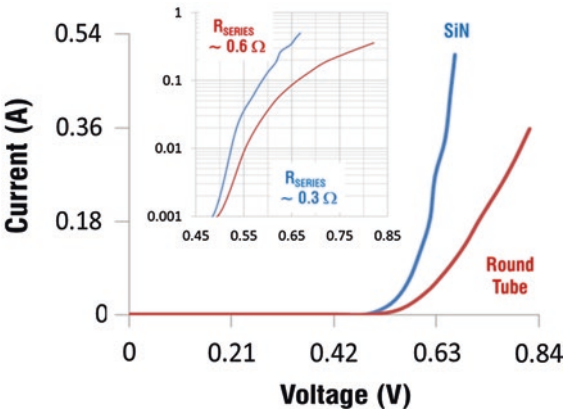

Fig. 5.17 Dark I-V measurements from processed solar cells at optimum temperature profile, in round tube furnace, exhibiting higher series resistance; inset in the graph plots the same measurements at logarithmic scale; for reference, I-V response from 18% solar cell (blue line) has been included

Round Tube Furnace Anneal

Figure 5.17 illustrates dark IV response of Ag and Al contacts annealed simultaneously in round tube furnace described in Chap. 4. Comparison with 18% cell reveals that series resistance has increased by a factor of 2, while shunt resistance remains nominally the same. This may be attributed to lower annealing temperature. Therefore, this system is also unsuitable for simultaneous annealing of solar cell contacts.

In Chap. 4, it was determined that Ag contact formation was a sensitive function of temperature variation with rapid rate of change favoring superior contact formation. The comparison of diode responses in four configurations confirms this. Rate of temperature change is comparable in IR conveyor belt and parallel-plate configurations resulting in comparable series resistances. The rate of change in quartz and round tubes is significantly slower with the resulting increase in series resistances. Therefore, for these circularly symmetric annealing configurations to be effective, transit speed needs to be significantly faster for quartz tube and rate of temperature increase higher in round tube.

5.3 Summary

Dark I-V measurements based on simple and inexpensive experimental configuration have been demonstrated to be highly effective in characterization of a wide range of screen-printed Ag and Al ohmic and rectifying contacts on n- and p-doped Si wafers. Experimental data is in good agreement with PC1D simulations as well industrially produced mc-Si and c-Si solar cells with SiN anti-reflection films operating at efficiencies in 14–18% range.

References

1. R. Handy, Solid State Electron. **10**, 765 (1967)
2. M. Wolf, H. Rauschenbach, Adv. Energy Convers. **3**, 455 (1963)
3. C. Fang and J. Hauser, 13th IEEE PVSC (1978)
4. L.D. Nielsen, IEEE Trans. Elec. Dev. **29**, 821 (1982)
5. M. Hamdy, R. Call, Solar Cells **20**, 119 (1987)
6. A. Kaminski, J.J. Marchand, A. Fave, A. Langier, 26th IEEE PVSC **203** (1997)
7. E.Q.B. Macabebe, E.E. Van Dyk, S. Afr. J. Sci. **104**, 401 (2008)
8. K. Bouzidi, M. Chegaar, M. Aillerie, Energy Procedia **18**, 1601 (2012)
9. A. Ortiz-Conde, F.J. García-Sánchez, J. Muci, A. Sucre-González, Facta Universitatis. Electron. Energetics **1**, 57 (2014)